Silicon photonic devices and platforms for the mid-infrared

M. Nedeljkovic,[1] A. Z. Khokhar,[1] Y. Hu,[1] X. Chen,[1] J. Soler Penades,[1] S. Stankovic,[1] H. M. H. Chong,[2] D. J. Thomson,[1] F. Y. Gardes,[1] G. T. Reed,[1] and G. Z. Mashanovich,[1,*]

[1]*Optoelectronics Research Centre, University of Southampton, Southampton, Hampshire, SO17 1BJ, UK*
[2]*Electronics and Computer Science, University of Southampton, Southampton, Hampshire, SO17 1BJ, UK*
[*]*g.mashanovich@soton.ac.uk*

Abstract: Due to its excellent electronic and photonic properties, silicon is a good candidate for mid-infrared optoelectronic devices and systems that can be used in a host of applications. In this paper we review some of the results reported recently, and we also present several new results on mid-infrared photonic devices including Mach-Zehnder interferometers, multimode interference splitters and multiplexers based on silicon-on-insulator, polysilicon, suspended silicon, and slot waveguide platforms.

OCIS codes: (160.3130) Integrated optics materials; (230.7370) Waveguides; (250.5300) Photonic integrated circuits.

References and links

1. L. Vivien and L. Pavesi, *Handbook of Silicon Photonics* (CRC Press, 2013).
2. www.luxtera.com
3. www.kotura.com
4. L. Vivien, A. Polzer, D. Marris-Morini, J. Osmond, J.-M. Hartmann, P. Crozat, E. Cassan, C. Kopp, H. Zimmermann, and J.-M. Fédéli, "Zero-bias 40Gbit/s germanium waveguide photodetector on silicon," Opt. Express **20**(2), 1096–1101 (2012).
5. G. Roelkens, L. Liu, D. Liang, R. Jones, A. Fang, B. Koch, and J. Bowers, "III-V/Silicon photonics for on-chip and intra-chip optical interconnect," Laser and Photonics Reviews **4**(6), 751–779 (2010).
6. J. S. Orcutt, B. Moss, C. Sun, J. Leu, M. Georgas, J. Shainline, E. Zgraggen, H. Li, J. Sun, M. Weaver, S. Urošević, M. Popović, R. J. Ram, and V. Stojanović, "Open foundry platform for high-performance electronic-photonic integration," Opt. Express **20**(11), 12222–12232 (2012).
7. R. Soref, "Mid-infrared photonics in silicon and germanium," Nat. Photonics **4**(8), 495–497 (2010).
8. M. M. Milošević, D. J. Thomson, X. Chen, D. Cox, and G. Z. Mashanovich, "Silicon waveguides for the 3-4 µm wavelength range," in *Proceedings of the 8th IEEE Conference on Group IV Photonics* (Institute of Electrical and Electronics Engineers, New York, 2011), pp. 208–210.
9. T. Baehr-Jones, A. Spott, R. Ilic, A. Spott, B. Penkov, W. Asher, and M. Hochberg, "Silicon-on-sapphire integrated waveguides for the mid-infrared," Opt. Express **18**(12), 12127–12135 (2010).
10. F. Li, S. D. Jackson, C. Grillet, E. Magi, D. Hudson, S. J. Madden, Y. Moghe, C. O'Brien, A. Read, S. G. Duvall, P. Atanackovic, B. J. Eggleton, and D. J. Moss, "Low propagation loss silicon-on-sapphire waveguides for the mid-infrared," Opt. Express **19**(16), 15212–15220 (2011).
11. A. Spott, Y. Liu, T. Baehr-Jones, R. Ilic, and M. Hochberg, "Silicon waveguides and ring resonators at 5.5 µm," Appl. Phys. Lett. **97**(21), 213501 (2010).
12. R. Shankar, I. Bulu, and M. Lončar, "Integrated high-quality factor silicon-on-sapphire ring resonators for the mid-infrared," Appl. Phys. Lett. **102**(5), 051108 (2013).
13. R. Shankar, I. Bulu, R. Leijssen, and M. Lončar, "Study of thermally-induced optical bistability and the role of surface treatments in Si-based mid-infrared photonic crystal cavities," Opt. Express **19**(24), 24828–24837 (2011).
14. G. Z. Mashanovich, M. M. Milošević, M. Nedeljkovic, N. Owens, B. Xiong, E.-J. Teo, and Y. Hu, "Low loss silicon waveguides for the mid-infrared," Opt. Express **19**(8), 7112–7119 (2011).
15. E. J. Teo, A. A. Bettiol, M. B. H. Breese, P. Y. Yang, G. Z. Mashanovich, W. R. Headley, G. T. Reed, and D. J. Blackwood, "Three-dimensional control of optical waveguide fabrication in silicon," Opt. Express **16**(2), 573–578 (2008).
16. P. Y. Yang, G. Z. Mashanovich, I. Gomez-Morilla, W. R. Headley, G. T. Reed, E. J. Teo, D. J. Blackwood, M. B. H. Breese, and A. A. Bettiol, "Free standing waveguides in silicon," Appl. Phys. Lett. **90**(24), 241109 (2007).
17. S. Khan, J. Chiles, and S. Fathpour, "Silicon-on-nitride waveguides for mid- and near-infrared integrated photonics," Appl. Phys. Lett. **102**(12), 121104 (2013).
18. R. A. Soref, S. J. Emelett, and W. R. Buchwald, "Silicon waveguided components for the long-wave infrared region," J. Opt. A, Pure Appl. Opt. **8**(10), 840–848 (2006).

19. M. Milošević, P. S. Matavulj, P. Y. Yang, A. Bagolini, and G. Z. Mashanovich, "Rib waveguides for mid-infrared silicon photonics," J. Opt. Soc. Am. B **26**(9), 1760–1766 (2009).
20. M. M. Milošević, M. Nedeljkovic, T. M. Ben Masaud, E. Jaberansary, H. M. H. Chong, N. G. Emerson, G. T. Reed, and G. Z. Mashanovich, "Silicon waveguides and devices for the mid-infrared," Appl. Phys. Lett. **101**(12), 121105 (2012).
21. M. Muneeb, X. Chen, P. Verheyen, G. Lepage, S. Pathak, E. Ryckeboer, A. Malik, B. Kuyken, M. Nedeljkovic, J. Van Campenhout, G. Z. Mashanovich, and G. Roelkens, "Demonstration of silicon-on-insulator mid-infrared spectrometers operating at 3.8μm," Opt. Express **21**(10), 11659–11669 (2013).
22. Z. Cheng, X. Chen, C. Y. Wong, K. Xu, C. K. Fung, Y. M. Chen, and H. K. Tsang, "Focusing subwavelength grating coupler for mid-infrared suspended membrane waveguide," Opt. Lett. **37**(7), 1217–1219 (2012).
23. F. Dell'Olio and V. M. Passaro, "Optical sensing by optimized silicon slot waveguides," Opt. Express **15**(8), 4977–4993 (2007).
24. Z. Wang, N. Zhu, Y. Tang, L. Wosinski, D. Dai, and S. He, "Ultra-compact low-loss coupler between strip and slot waveguides," Opt. Lett. **34**(10), 1498–1500 (2009).
25. Z. Cheng, X. Chen, C. Y. Wong, K. Xu, and H. K. Tsang, "Mid-infrared suspended membrane waveguide and ring resonator on silicon-on-insulator," IEEE Phot. J. **4**(5), 1510–1519 (2012).
26. C. Reimer, M. Nedeljkovic, D. J. M. Stothard, M. O. S. Esnault, C. Reardon, L. O'Faolain, M. Dunn, G. Z. Mashanovich, and T. F. Krauss, "Mid-infrared photonic crystal waveguides in silicon," Opt. Express **20**(28), 29361–29368 (2012).
27. D. J. Thomson, F. Y. Gardes, J.-M. Fedeli, S. Zlatanovic, Y. Hu, B. P.-P. Kuo, E. Myslivets, N. Alic, S. Radic, G. Z. Mashanovich, and G. T. Reed, "50 Gbit/s silicon optical modulator," IEEE Photon. Technol. Lett. **24**(4), 234–236 (2012).
28. Y. Hu, R. M. Jenkins, F. Y. Gardes, E. D. Finlayson, G. Z. Mashanovich, and G. T. Reed, "Wavelength division (de)multiplexing based on waveguide mode dispersion," Opt. Lett. **36**(23), 4488–4490 (2011).
29. D. J. Thomson, Y. Hu, G. T. Reed, and J.-M. Fedeli, "Low loss MMI couplers for high performance MZI modulators," IEEE Photon. Technol. Lett. **22**(20), 1485–1487 (2010).
30. W. Bogaerts, S. K. Selvaraja, P. Dumon, J. Brouckaert, K. De Vos, D. Van Thourhout, and R. Baets, "Silicon-on-insulator spectral filters fabricated with CMOS technology," IEEE J. Sel. Top. Quant. **16**(1), 33–44 (2010).
31. Y. Wei, G. Li, Y. Hao, Y. Li, J. Yang, M. Wang, and X. Jiang, "Long-wave infrared 1 × 2 MMI based on air-gap beneath silicon rib waveguides," Opt. Express **19**(17), 15803–15809 (2011).
32. D. J. Thomson, F. Y. Gardes, Y. Hu, G. Mashanovich, M. Fournier, P. Grosse, J.-M. Fedeli, and G. T. Reed, "High contrast 40Gbit/s optical modulation in silicon," Opt. Express **19**(12), 11507–11516 (2011).
33. M. Nedeljkovic, R. Soref, and G. Z. Mashanovich, "Free-carrier electrorefraction and electroabsorption modulation predictions for silicon over the 1-14μm infrared wavelength range," IEEE Photonics J. **3**(6), 1171–1180 (2011).
34. M. A. Van Camp, S. Assefa, D. M. Gill, T. Barwicz, S. M. Shank, P. M. Rice, T. Topuria, and W. M. Green, "Demonstration of electrooptic modulation at 2165nm using a silicon Mach-Zehnder interferometer," Opt. Express **20**(27), 28009–28016 (2012).
35. Y. Hu, F. Y. Gardes, D. J. Thomson, G. Z. Mashanovich, and G. T. Reed, "Coarse wavelength division (de)multiplexer using interleaved angled multimode interferometer structure," Appl. Phys. Lett. **102**(25), 251116 (2013).

1. Introduction

There has been remarkable progress in silicon photonics in the last 10 years. Driven by the interconnect bottleneck problem and leveraging the mature microelectronics technology, researchers in academia and industry have reported many breakthroughs [1] that have led to the first commercial silicon photonics products [2,3].

The most dominant platform for datacom and telecom applications has been silicon-on-insulator (SOI) with typical silicon overlayer thicknesses in the range 200-400 nm. Both Si and SiO$_2$ are low loss in the near-infrared (NIR). Also, germanium can be used for efficient photodetection [4]. As an indirect semiconductor, silicon is not suitable as a material for light sources and therefore III-V/Si hybrid integration has been successfully developed to solve this problem [5]. Recently, much effort has been devoted to the integration of photonic and electronic circuits on the same chip [6].

Silicon is transparent not only in the NIR but also up to ~8 μm and is potentially a viable material for mid-infrared (MIR) applications. In the last few years, there has been an increased interest in silicon-based MIR materials and photonic devices. The MIR is a spectral region of tremendous scientific and technological interest. Spanning a large wavelength range, it contains strong vibrational signatures for a number of gases and molecules, and hence photonic devices that operate in this region can be potentially applied for a host of applications in environmental and bio-chemical sensing, defence and security, medicine, industrial control, astronomy, and also in communications. A common requirement for MIR

passive photonic devices is low loss. For active devices low loss and high efficiency are required, however other parameters can vary depending on the application. For example, high speed modulators would be needed for MIR communications, whilst moderate speeds are sufficient for sensing applications.

Optical properties of materials reported in the literature [7] suggested that SOI could not be used between 2.6 and 2.9 μm and beyond 3.6 μm due to the large absorption of SiO_2. We have investigated SOI devices in the 3-4 μm range and our findings are presented in this paper. As the absorption of SiO_2 is the main limitation of SOI for longer MIR wavelengths, alternative platforms have also been evaluated.

As sapphire is transparent up to ~5.5 μm, silicon-on-sapphire (SOS) waveguiding at 3.4, 4.4, 5.08, and 5.5 μm has been reported in the last three years [8–11]. Propagation losses of 3.6 dB/cm at 3.4 μm, 4.3 dB/cm at 4.5 μm, 1.9 dB/cm at 5.08 μm, and 4 dB/cm at 5.5 μm for SOS waveguides have been achieved. SOS ring resonators of 40 μm radius revealed Q-values up to 3,000 in the wavelength range of 5.4-5.6 μm [11]. Recently, Shankar et al. reported SOS ring resonators at 4.3-4.6 μm with Q factors in excess of 150,000 [12]. To improve the Q factor and reduce the loss, the authors used Piranha etch/HF cycling and annealing [13]. Researchers have used both in-plane and out-of-plane coupling of optical fibres with SOS waveguides. For in-plane coupling, preparation of the waveguide facets can be problematic as sapphire is difficult to polish and is usually cleaved, resulting in variable facet quality. We have previously reported FIB trimming of SOS waveguide facets to improve their optical quality [8].

By replacing the silicon dioxide with a different cladding, we can potentially obtain structures that are less lossy at longer MIR wavelengths. One such cladding material is porous silicon. Fabrication of silicon on porous silicon (SiPSi) waveguides by proton beam irradiation has recently been reported [14]. Ion irradiation with 250 keV protons and a fluence of approximately 1×10^{14} cm^{-2}, with a subsequent two-step electrochemical etching in a solution of HF:water:ethanol was used. This resulted in a Si strip waveguide core on the annealed porous Si cladding with s refractive index that depends on the porosity and can be as low as 1.4 [14]. The porous silicon can be selectively etched to form a "mushroom" shaped waveguide with an air cladding and a narrow stem to retain connection with the substrate [15]. Also, two-step proton implantation process can be used to form silicon suspended waveguides [16].

Very recently, Khan et al. reported 2 μm high rib silicon on silicon nitride (SON) waveguides, with a propagation loss of 5.2 dB/cm at 3.39 μm [17]. The waveguides were fabricated by bonding a silicon die to an SOI die coated with a low-stress silicon nitride layer. The SOI substrate was subsequently removed resulting in an SON platform. As silicon nitride is transparent up to approximately 7 μm [7], and has relatively low refractive index of ~2, this platform can potentially offer realization of compact MIR silicon devices for a large wavelength band.

This paper is organized as follows: SOI based waveguides are presented in section 2, section 3 and 4 show recent results for multimode interference splitters and Mach-Zehnder interferometers realized in different platforms, whilst section 5 introduces a novel MIR multiplexer structure.

2. SOI based waveguides

Due to mature fabrication processes and significant improvements achieved in the material quality over the last 20 years, SOI is a desirable photonic material platform in terms of technology transfer from the NIR to MIR. The platform has been investigated in the MIR first theoretically [18,19] and subsequently, experimentally. We have reported propagation losses of 0.6-0.7 dB/cm at 3.39 μm for both TE and TM polarizations in 2 μm rib SOI waveguides [14]. In 2012 and 2013, 500 nm and 400 nm thick strip SOI waveguides with losses in the 3-5 dB/cm range at 3.8 μm were reported [20, 21]. Rib waveguides with similar thicknesses can also be used for the fabrication of MIR optical modulators or suspended waveguides, where

the buried oxide cladding is selectively removed by undercutting the rib [22]. In the following sub-sections, we report our recent results for rib, slot, suspended and polysilicon waveguides.

2.1 Small SOI rib waveguides

Compact photonic devices can be realized using small rib waveguides as they can have tight bends. Our rib waveguide patterns were written using a JEOL JBX 9300FS e-beam lithography tool on 6-inch SOI wafers. ZEP-520A, a non-chemically amplified high resolution positive resist from Nippon Zeon, was used. Patterns in ZEP-520A were transferred to the SOI wafers by inductively coupled plasma (ICP) etching using an Oxford Instruments ICP 380 plasma system. The fabrication tolerance for the waveguide width and etch depth was $\pm$ 10 nm, and was taken into account during the design stage for various devices presented here. The simulations were performed using Photon Design Fimmwave software package with complex FMM solver.

The waveguides were 400 nm high with 220 nm etch depth and 2000 nm of buried oxide (BOX). The width was varied from 1 to 1.35 μm. The experimental setup described in [14] was used to characterize the waveguides, as well as other devices presented in this paper. The cut back method was used to estimate the propagation loss. It was performed by measuring transmission through straight waveguides with lengths varying between 0.1 and 0.9 cm. The grating couplers were 20 μm wide and 50 μm long, and were connected to single mode waveguide sections by 1 mm long tapers. Figure 1 shows cut back loss measurement for 400 nm × 1350 nm rib SOI waveguides at a wavelength of 3.77 μm. The propagation loss was determined to be 1.46 $\pm$ 0.20 dB/cm, which is the lowest value obtained in this wavelength range to date. Further loss reduction may be possible by smoothing the waveguide sidewalls, as demonstrated for waveguides operating in the NIR.
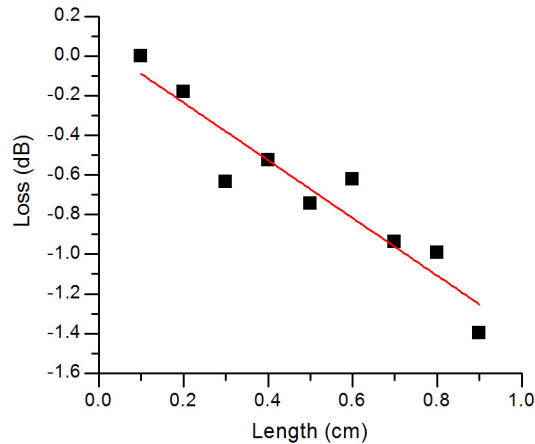

Fig. 1. Cut back propagation loss measurement for 400nm × 1350nm rib SOI waveguides.

2.2. Slot waveguides

For increased sensitivity of future MIR silicon photonic sensors, a slot waveguide can be used as it can enhance the electric fields amplitude in the gap region (up to 20 × higher) as compared to standard waveguide structures. A detailed modal and sensitivity description of this structure in the NIR can be found in [23]. In this sub-section we report the first realization of MIR slot waveguides in silicon. The simulation for the whole structure, including the coupler and slots, was performed using Photon Design Fimmprop with complex FMM solver and 200 × 200 mode profile resolution. We have also used other methods like the FEM to check validity of the results.

The coupling of light in and out of the chip has been achieved by adding rib waveguides at the input and the output, terminating both with a taper, and finishing each side of the

conductors of the slot in tapers overlapping the rib taper, as can be seen in Fig. 2. The idea for this design was adapted from [24]. Grating couplers were added at the end of the ribs for coupling to/from optical fibers. We focused our simulations on a gap size between 100 nm and 140 nm as the confinement factor was drastically reduced for gaps larger than 150 nm.

The devices were fabricated on 6-inch SOI wafers with 400 nm Si on 2 μm BOX using e-beam lithography and ICP etching. The slot width, the gap in the interface region, and the length of slot waveguides were varied. The rib and slot waveguides, as well as the grating couplers were fabricated with a 220 nm etch depth, hence the entire fabrication process was performed by a single etch step. By cascading different numbers of pairs of rib-slot transitions (Fig. 2) and plotting a line of best fit between the plotted outputs, we determined that a 100 nm gap in the rib-slot transition showed a loss of 0.04 dB/interface, whilst the loss was 0.06 dB/interface for a gap of 130 nm. The propagation loss for slot waveguides with the total width of 1.42 μm and slot width of 100-140 nm was 9-10 dB/cm. Future work will include the reduction of the propagation loss by designing slightly wider waveguides, smoothing the sidewalls and by a further reduction of the gap in order to optimize the performance and minimize the loss.
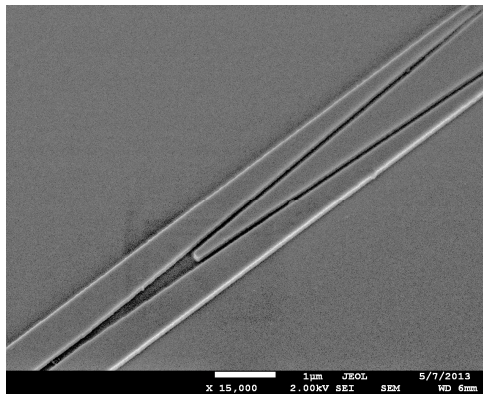

Fig. 2. SEM image of a rib-slot waveguide interface.

2.3. Poly Si waveguides

Amorphous and polysilicon have been investigated in the last several years for back-end processing and fabrication of multilayer integrated circuits. As polysilicon can offer flexibility in terms of waveguide layer thickness and therefore offers the possibility of both NIR and MIR circuits on the same chip, we have investigated the waveguide structure shown in Fig. 3. The waveguides were fabricated using the imecAP process [21]: 5 nm of thermal SiO_2 was grown on 220 nm SOI with 2 μm of buried oxide. Subsequently 160 nm of amorphous Si (a-Si) was deposited using Low Pressure Chemical Vapour Deposition (LPCVD). On top of the a-Si, 10 nm of SiO_2 and 70 nm of SiN were deposited using PECVD. The SiN layer served as a hard mask for waveguide etching. The stack was subsequently annealed at 750°C for 30 minutes to convert the a-Si to polySi. This step was performed to increase the temperature budget for eventual post-processing on the silicon wafer. The waveguides were fabricated using 193 nm DUV lithography and halogen based dry etching. The rib waveguides had the following dimensions: H = 380 nm, D = 200 nm and W = 1100 nm (Fig. 3).
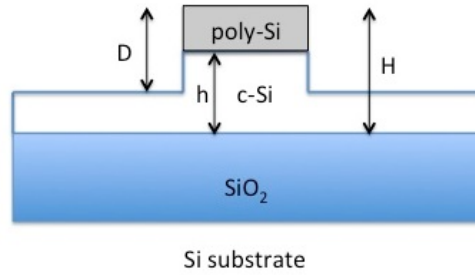
Fig. 3. Schematic of a poly Si-on-SOI waveguide.

The cut back method was used to measure the propagation loss of these waveguides. At a wavelength of 3.76 μm we have measured a propagation loss of 7.5 ± 0.1 dB/cm. The loss can be reduced to ~5.3 dB/cm by using a shallower etch and wider waveguides as shown in [21]. We attribute the larger loss than those obtained for the crystalline Si waveguides to the scattering loss in the polySi layer, due to grain boundaries.

2.4. Suspended waveguides

To extend the transmission of the SOI platform, suspended waveguides can be used. Cheng et al. designed and characterized 340 nm high Si rib waveguides with an undercut BOX, at a wavelength of 2.75 μm [22,25]. Deep holes were etched in a periodic pattern close to the rib waveguides, enabling removal of the BOX in HF solution. The holes were located far enough from the rib to have negligible interaction with the optical mode. A propagation loss of 3 dB/cm was measured at 2.75 μm.
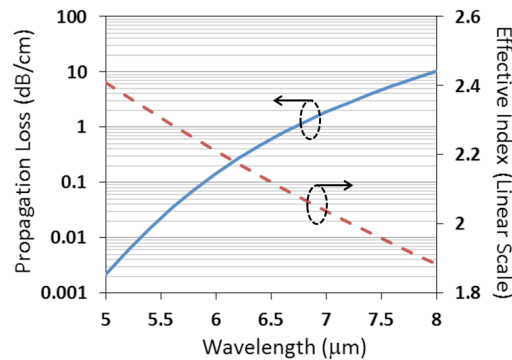

Fig. 4. Simulated effective index and propagation loss for 500 nm thick suspended rib waveguides with 150 nm etch depth, 5 μm width, and 3μm BOX.

We have theoretically investigated the transmission range of such waveguides. The simulations were performed by the Finite Element Method (FEM) with COMSOL Multiphysics software. Figure 4 shows the propagation loss and effective index of a waveguide with 500 nm top silicon layer and a 3 μm BOX thickness. Such waveguides can support wavelengths up to ~7 μm (Fig. 4). The BOX was assumed to be removed to form a membrane waveguide. The waveguide is 5 μm wide and has a 150 nm shallow-etch depth. These waveguide dimensions have been chosen to relax the lateral confinement of light, and therefore increase the vertical light confinement. We have only considered the substrate leakage in the simulations. The actual loss could be higher due to an additional contribution from scattering loss. It is worth mentioning that an alternative approach utilizing MIR photonics crystals (PhC) platform has also been recently demonstrated [26].

3. Multimode interference splitters

Multimode interference (MMI) splitters are important devices that we have used in fast optical modulators [27] and in multiplexers [28]. Here, we report results for MMIs designed for 3.8 µm. MMIs were fabricated using e-beam lithography and ICP etching on both 400 nm and 500 nm SOI. The optimum design dimensions for the 400 nm structures were: W_{MMI} = 8 µm, L_{MMI} = 21.0 µm, S = 4.18 µm, W_{tap} = 2.6 µm, L_{tap} = 20 µm and for the 500 nm structures: W_{MMI} = 8 µm, L_{MMI} = 21.83 µm, W_{tap} = 3.0 µm, L_{tap} = 20 µm and S = 4.0 µm (Fig. 5).

Simulations performed with the Photon Design Fimmprop FMM complex solver predicted an insertion loss of 0.075dB due to mode mismatch. The insertion loss was measured by cascading different numbers of pairs of MMIs together (2-18), and plotting a line of best fit between the plotted outputs. The minimum measured insertion loss per MMI was determined to be 0.10 ± 0.01 dB at a wavelength of 3.8 µm (Fig. 6). The loss figure achieved is of similar magnitude to the lowest reported losses for MMIs at near-infrared wavelengths [29,30] and are much lower than previously reported values in the MIR [20,31]. The improvement in loss figures over [20] is attributed to fabrication improvements, so that device dimensions were much more closely matched to the designed dimensions.
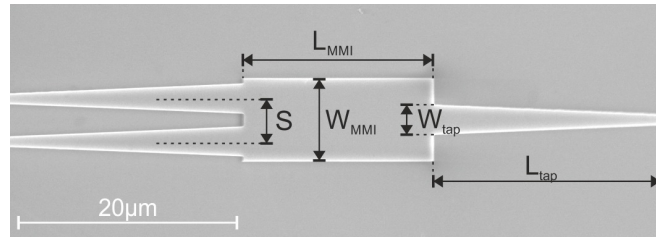

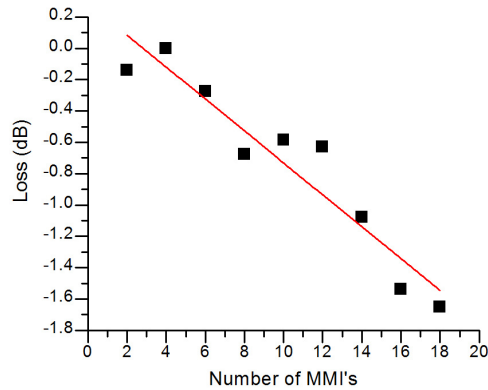Fig. 5. SEM image of a fabricated 1 × 2 MIR SOI MMI with tapered input and output ports.

Fig. 6. Insertion loss measurement for 400 nm thick SOI MIR MMIs.

To demonstrate that our design can be low loss for different material platforms we have designed MMIs based on the rib waveguide shown in Fig. 3. We have used identical measurement techniques to determine the insertion loss of MMIs based on polySi on SOI waveguides. We measured 0.37 ± 0.08 dB/MMI. This result is very close to those achieved for 400 and 500 nm SOI MMIs, thus demonstrating the viability of our design.

4. Mach-Zehnder interferometers

Mach-Zehnder interferometers (MZIs) are commonly used in silicon photonics as a key building block of modulators [27, 32–34], and are also used as wavelength filters. We have

fabricated asymmetric MZIs with one input and one output, with MMIs used as splitters and couplers.

In devices with both 400 nm and 500 nm thick Si layers the total MZI length of the shorter arm was 928 μm, and the arm length differences were 300 μm and 350 μm, respectively. The transmission spectra were normalized to that of a standard waveguide. The measured insertion loss over the 3.7-3.9 μm wavelength range was 1.6-2.4 dB, the maximum extinction ratio was between 27 dB and 34 dB, and the FSR around 10 nm. From the measured FSR we calculated a group index of 4.19, which matched well the simulated value of 4.03 obtained with Fimmwave. An unbalanced MZIs with PhC waveguides in one arm have been recently demonstrated and used for group index measurements [26].
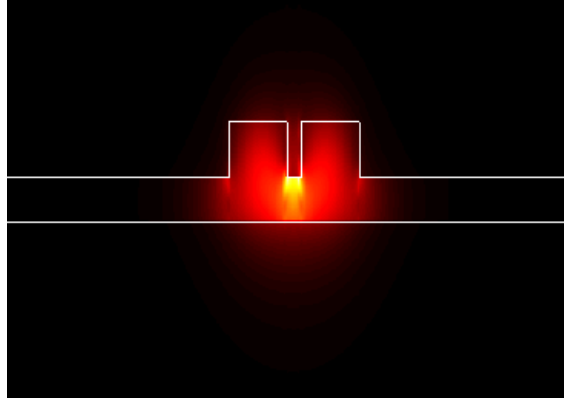

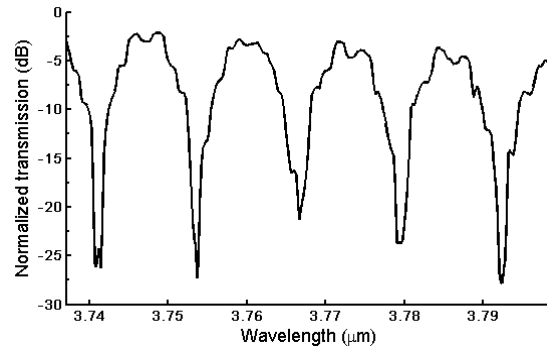Fig. 7. Cross sectional dimension of the slot waveguide.

Fig. 8. Response of a Mach-Zehnder asymmetric interferometer based on slot waveguides.

Here, we also report a MIR MZI based on slot waveguides, a structure that can be interesting for sensing applications. The MZI was based on the slot waveguide shown in Fig. 7. The dimensions were: W_{slot} = 660 nm, W_{gap} = 120 nm, W_{total} = 2 × W_{slot} + W_{gap} = 1440nm, H = 400 nm, and H_{slot} = 220 nm. Figure 8 shows the response from an asymmetric MZI with an arm length difference of 350 μm, and with a straight slot waveguide section 585 μm long. The rib-slot interface gap was 130 nm.

It is worth noting that because of the mode-hopping behavior of the commercial QCL used for these measurements it is difficult to interrogate fine wavelength features, and some of the peaks in the spectra appear to have multiple minima or were clipped.

5. Angled multimode interference multiplexer

Mulitplexers/demultiplexers are important photonic devices for future MIR high-speed datacom/telecom integrated circuits and sensors. The most popular approaches in the NIR have been Arrayed Waveguide Grating (AWG) and Planar Concave Grating (PCG, or echelle

grating) multiplexers. Recently, MIR spectrometers based on these structures have been reported [21].

We have experimentally demonstrated an alternative approach, a 4-channel and 8-channel angled multimode interferometer (AMMI) structures at around 1550 nm, for wavelength division (de)multiplexing [28,35]. The device has the distinct advantage of low insertion loss (<2 dB), low cross-talk (−20 dB), and ease of fabrication (single-step lithography and etching). The realization of a 3-channel AMMI for the mid-infrared applications is reported here.

The device is shown in Fig. 9. The input and output waveguides of width, W_{IO}, are tilted at an angle, θ, when accessing the multimode waveguide of width W_{AMMI}. The axial distance between the input and output waveguides for the ith output channel, L_i, is governed by the dispersive relation of self-imaging MMI, given by:

$$L_i = \frac{4 n_{eff,AMMI} \times W_{AMMI}^2}{\lambda_i}.$$ (1)

where, $n_{eff,AMMI}$ is the effective refractive index of the fundamental mode in the AMMI's multimode waveguide. The quality of spectral response, e.g. insertion loss and cross talk, is dependent on the structural parameters, which were optimised using a commercial simulation package, FIMMWAVE. The optimised parameters were: $W_{IO} = 28$ μm, $\theta = 26.4°$, $W_{AMMI} = 50$ μm, $L_1 = 5132$ μm, $L_2 = 5066$ μm, $L_3 = 5000$ μm.
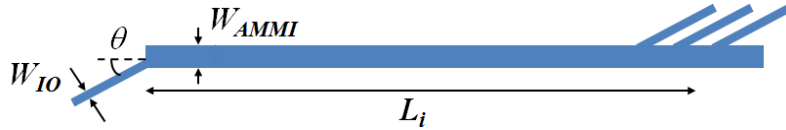

Fig. 9. Schematic of an AMMI.

The designed devices were patterned on a 6-inch SOI wafer with a silicon overlayer thickness of 400 nm and BOX thickness of 2 μm using single-step electron beam lithography. The pattern was transferred to the wafer using inductively coupled plasma (ICP) etching.

The measured spectral response of the fabricated device is shown in Fig. 10, which has a channel spacing of 30 nm, an insertion loss of about 4-5 dB and a cross talk of −12 dB. The measured data is subject to the stability of the MIR laser source. Whilst these values are slightly higher than those demonstrated in the NIR, one can see that the merits of the AMMI structure for WDM in the NIR wavelength range, e.g. low insertion loss and low cross-talk are maintained around the wavelength of 3.8 μm. Further work will focus on the reduction of the insertion loss and cross talk, and increasing the number of channels, using for example the approach already demonstrated in [35].
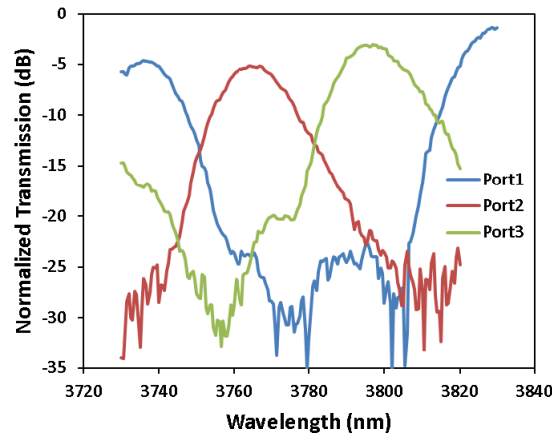
Fig. 10. Experimental response of a 3-channel MIR angled MMI.

6. Conclusions

Silicon is a very attractive platform for the MIR. We have shown that the SOI platform, so dominant in the NIR, with certain modifications, can be used in a wide range of wavelengths. Despite higher SiO_2 losses beyond 3.6 μm, we have demonstrated 400 nm high SOI waveguides with propagation losses as low as ~1.5 dB/cm, low insertion loss MMIs (0.1 dB/MMI), and high extinction ratio MZIs (25-30 dB), all at the wavelength of 3.8 μm. We have also, presented realization of the first MIR slot waveguides and interferometers based on such waveguides. Whilst the initial results show relatively high losses, loss reduction is possible by further optimization of the design. We have also demonstrated a 3-channel multiplexer based on an AMMI, with insertion losses in the range of 4-5 dB and cross talk of −12 dB. The number of channels can be increased by the implementation of the interleaved AMMI design. These results together with the demonstration of the polysilicon platform that offers significant design flexibility, with a possibility to further expand the transmission range by implementing undercut structures, give a solid base for the development of MIR silicon integrated photonic circuits for a range of applications.